Progress in Biomaterials (2022) 11:263–271
https://doi.org/10.1007/s40204-022-00193-8

ORIGINAL RESEARCH

Influence of alumina substrates open porosity on calcium phosphates formation produced by the biomimetic method

Isabela R. Lavagnini[1] · João V. Campos[1] · Denise Osiro[1] · Julieta A. Ferreira[1] · Luiz A. Colnago[2] · Eliria M. J. A. Pallone[1,3]

Received: 1 April 2022 / Accepted: 3 June 2022 / Published online: 23 June 2022

Abstract
We evaluated the influence of the open porosity of alumina (Al_2O_3) substrates on the phase formation of calcium phosphates deposited onto it surface. The Al_2O_3 substrates were prepared with different porosities by the foam-gelcasting method associated with different amounts of polyethylene beads. The substrates were coated biomimetically for 14 and 21 days of incubation in a simulated body fluid (SBF). Scanning electron microscopy characterisation and X-ray computed microtomography showed that the increase in the number of beads provided an increase in the open porosity. The X-ray diffraction and infrared spectroscopy showed that the biomimetic method was able to form different phases of calcium phosphates. It was observed that the increase in the porosity favoured the formation of β-tricalcium phosphate for both incubation periods. The incubation period and the porosity of the substrates can influence the phases and the amount of calcium phosphates formed. Thus, it is possible to target the best application for the biomaterial produced.

Keywords Al_2O_3 · Porous ceramic · Biomimetic coating · Calcium phosphates

Introduction

Aluminium oxide (Al_2O_3) is a ceramic material with great potential for use as a biomaterial in bone implants. In addition to its bioinert nature, Al_2O_3 can be shaped into a porous structure and still have excellent mechanical properties (Rambo et al. 2006; Böke et al. 2014; Toccafondi et al. 2015; Salerno et al. 2016; Silva et al. 2019). However, it is important to note that bioinert implants, when inserted into the body, are encapsulated by fibrous tissues (Abe et al. 1990). These fibrous tissues isolate the implant from the surrounding bones, which minimises its proper functioning (Abe et al. 1990; Kolos and Ruys 2015; Hesaraki 2016).

To avoid the formation of fibrous tissues around bioinert materials, Abe et al. (1990) developed a method that allows the activation of a bioinert surface, increasing its biological activity. The activation occurs by the formation of a bioactive ceramic layer on a material surface from its immersion in a blood plasma simulating solution (SBF—simulated body fluid) (Barrere et al. 2002a, b). Thus, this biomimetic coating allows the combination of bioactivity on the surface of a bioinert material (Kokubo 1998; Rambo et al. 2006; Dorozhkin 2012; Böke et al. 2014; Kolos and Ruys 2015; Tang et al. 2016; Sartori et al. 2018; Silva et al. 2018; Nunes et al. 2021).

The bioactive surface formed in the bioinert material from the biomimetic coating consists of different phases of calcium phosphates. The most common are: hydroxyapatite (HA), α- and β-tricalcium phosphates (α-TCP, β-TCP), tetracalcium phosphate (TTCP), and octacalcium phosphate (OCP) (dos Santos et al. 2017, 2018; Sartori et al. 2018; Silva et al. 2019; Nunes et al. 2021; Karampouret al. 2022).

Calcium phosphates presents high similarity with the mineral part of the bones. The period of time that calcium phosphates remain in the body depends on its phase.

✉ Isabela R. Lavagnini
isabela.lavagnini@usp.br

[1] Postgraduate Programme in Materials Science and Engineering, University of São Paulo, USP/FZEA, Av. Duque de Caxias Norte, 225, Pirassununga, SP 13635-900, Brazil

[2] Brazilian Agricultural Research Corporation, EMBRAPA Instrumentation, Rua Quinze de novembro, 1500/1501, São Carlos, SP 13561-206, Brazil

[3] Department of Biosystem Engineering, Faculty of Animal Science and Food Engineering (FZEA), University of São Paulo (USP), Pirassununga, SP 13635-900, Brazil

Degradation rate of each phase in the physiological environment can influence the osteoconduction and osteoinduction properties of the biomaterial, indicating in which application it will be best used (Shavandi et al. 2015; Hesaraki 2016; Ebrahimi et al.2017; Seyedlar et al. 2019; Bohner et al. 2020).

Some modifications in the surface of the bioinert substrates, made before coating, can lead to improvements in the formation of the biomimetic layer (Belwanshi et al. 2021). These changes may be physical (i.e. changes in the roughness, surface energy, and surface area of the material Faga et al. 2012; dos Santos et al. 2017; Sartori et al. 2018; Santos et al. 2020)) or chemical (i.e. the activation of functional sites that favour the deposition of phosphates Uchida et al. 2002; Dehestani et al. 2012; Silva et al. 2018)). These changes can influence the formation rate, thickness, and adhesion between the calcium phosphates formed with the modified surface of the bioinert material (Faga et al. 2012; Böke et al. 2014; dos Santos et al. 2017; Bohner et al. 2020; Belwanshi et al. 2021).

The presence, quantity, morphology, and interconnectivity of pores are the main characteristics to consider for the use of this biomaterial as a bone replacement (Sabree et al. 2015). These porous biomaterials must have inter-connected pores (open pores) to promote tissue growth inside them, improving their biological fixation (Thavornyutikarn et al. 2014; Kolos and Ruys 2015; Hesaraki 2016). Also, regenerative behaviour and bone tissue formation can occur in different ways according to specific pore diameter ranges (Annabi et al. 2010; Chen et al. 2012). There is several methods to produce porous materials, e.g. anodization (Toccafondi et al. 2015; Karczewski et al. 2017), replica method (Silva et al. 2018), sacrifice material (e.g. polymers, agricultural wastes) (Dele-Afolabi et al. 2017, 2018a, b,2021) and foam gelcasting (Xie et al. 2012; Salomão et al. 2014), to list a few.

Therefore, we evaluated the influence of the Al_2O_3 substrates open porosity on the phase formation of calcium phosphates obtained by the biomimetic method.

Experimental

The Al_2O_3 commercial powder used in the preparation of the substrates was CT-3000SG, from Alcoa & Chemicals Ltd., 99.8% pure and with an average particle size of 0.5 µm. The substrates were prepared using the foam-gelcasting method without a controlled atmosphere (Petit et al. 2016; Sartori et al. 2018) adding a secondary organic phase, which was eliminated during calcination. The secondary organic phase used was polyethylene (PE) beads (200 ± 50 µm average diameter). The beads were added in the final stage of processing in proportions of 0, 5, 10, and 15% by weight to increase the porosity of the final material. The gel formed was deposited in Petri dishes. The samples were then calcined at 600 °C for 2 h (5 °C min^{-1}), and sintered at 1500 °C for 2 h (10 °C min^{-1}). After sintering, the samples were cut into cylindrical shapes with 10 mm diameter and 3 mm height. According to the mass percentage of PE beads initially added (0, 5, 10, and 15%), the samples were named A0PE, A5PE, A10PE, and A15PE.

The structures and surfaces of the substrates were evaluated before coating using a scanning electron microscope (SEM; HITACHI TM 3000). The distribution, pore size, and open porosity were determined by X-ray computed microtomography (µCT; SKY SCAN 1172). CT-Analyzer software was used to treat the experimental data generated by µCT. The tensile strength by diametral compression test (Brazilian Test) was obtained according to ASTM D3967-16a (ASTM D3967-95a 2001). For that a universal mechanic testing (MTS 370.02) was used with a head velocity of 1 mm min^{-1} at a temperature of 25 °C. The tensile stress (σ) versus strain (ε) curves were analysed for at least 10 cylindrical samples per condition. The samples diameter was sized twice its height (10 × 5 mm, respectively).

The biomimetic coating was carried out according to the procedure proposed by Barrere et al. (2002a). In this procedure, the concentration of the SBF solution is 5 × higher than the SBF solution originally proposed by Abe et al. (1990). After the 14- and 21-day incubation periods, at 36.5 °C, under constant agitation (60 rpm), the covered substrates were washed with distilled water and dried at 50 °C for 24 h. It should be noted that the SBF 5 × solution was renewed every 72 h and the pH of the medium was adjusted to 6.1 with hydrochloric acid at a concentration of 1 $molL^{-1}$ (Barrere et al. 2002b; dos Santos et al. 2017; Sartori et al. 2018).

After the biomimetic coating, the calcium phosphate formed was analysed by SEM (HITACHI TM 3000). The crystalline phases were characterised by X-ray diffraction (XRD; RIGAKU MINIFLEX 600), in the range of 27º–34º, and a step of 0.20º. For this purpose, the analytical diffractogram deconvolution curves were obtained using the Gaussian function ($R^2 > 0.99$), with the Savitsky–Golay filter, using Origin 2019 software from OriginLab Corporation. The mathematical procedure was used to a semi-quantitative interpretation of the different phases of calcium phosphates formed during the biomimetic coating. The displacements of the X-ray curves were based on the standard Miller indices (hkl) for each phase of calcium phosphate, according to the database provided by the Joint Committee for Powder Diffraction Studies (JCPDS) (Gadaleta et al. 1996; dos Santos et al. 2017; Sartori et al. 2018; Santos et al. 2020).

The calcium phosphates formed on the surfaces of the substrates were quantified by spectroscopy in the near-infrared region (NIR; Perkin Elmer, model Spectrum 100 N, with diffuse reflectance accessory, NIRA), from 32 spectra and a resolution of 16 cm^{-1}. The spectra were mathematically

treated for correction of the baseline, obtaining the second derivative to locate the vibration peaks, and deconvolution with signal adjustment, to calculate the area of the absorption bands. In deconvolution, the Gaussian function ($R^2 > 0.98$) and the Savitsky–Golay filter were used, using Origin 2019 software from OriginLab Corporation as previously reported.

The Al_2O_3 substrates (without calcium phosphate deposition) were used as a reference spectrum for assigning its characteristic bands. In the spectra obtained from substrates with deposited calcium phosphate, the bands assigned to alumina were used as a reference, being normalised to allow the quantification of phosphates (Sartori et al. 2018). Thus, the total area of the normalised spectra will vary with respect to the amount of phosphates deposited. To quantify the phosphates formed, the region between 5430 and 4630 cm^{-1} of the NIR spectrum was analysed. This combination region was chosen because it has absorptions attributed to phosphate groups and the surface of alumina, with less interference from adsorbed water signals. Furthermore, the substrates were previously dried at 100 °C for 24 h to remove excess surface moisture (Czarnik-Matusewiczet al. 2005; Brangule and Gross 2015; Kolmas et al. 2015; Sartori et al. 2018).

The relationship between the different phases of calcium phosphates and the porosity of the samples was analysed by Pearson's correlation coefficient (r), and the statistical significance was considered at $p < 0.05$, using Origin 2019 software from OriginLab Corporation.

Results and discussion

Characterisation of Al_2O_3 substrates

Figure 1 shows the open porosity obtained by μCT and the tensile strength of the Al_2O_3 substrates with different additions of PE beads. In general, the increase in the secondary organic phase increased the open porosity of the substrates.

Although different amounts of PE beads added produce similar open porosity results, when we compare them with the A0PE condition, it is clear that the addition of beads increases the open porosity. The addition of PE beads may have increased this open porosity by settling on the pore walls provided by the foam-gelcasting method. Therefore, the addition of PE beads would contribute to the formation of an open path between the pores, thus providing greater interconnectivity. Similarly, Karczewski et al. also showed that adding a small quantity (5% by wt) of an organic compound resulted in an improvement in the pores interconnectivity when compared with the same substrate without the addition of the organic compound. The interconnectivity between the pores and their spatial distributions in the

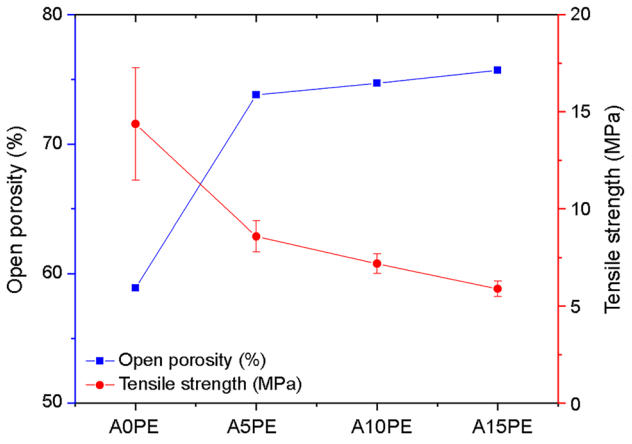

Fig. 1 Open porosity and tensile strength of substrates with different additions of PE (the lines are just a guide for the eyes)

substrate structure is of great importance, as they allow for several biological activities necessary for better functioning of the implant, in addition to improving its fixation (Karageorgiou and Kaplan 2005; Yoo 2013; Sabree et al. 2015; Arabnejad et al. 2016; Wang 2016).

Despite the importance of the interconnectivity between the pores, one should consider that the mechanical strength would decrease with the increase in porosity (Dele-Afolabi et al. 2017; Xu et al. 2019). Compressive strength is the most commonly used parameter to evaluate the mechanical properties of a bone replacement biomaterial (Zhang et al. 2014; Schröter et al. 2020). However, brittle materials tend to have considerably lower tensile strength and shear strength in relation to their compressive strength. Thus, brittle materials are most likely to fail when they are under tension, which can render them susceptible to fatigue failure by cyclic loading over long-term implantation in human bone (Canal and Ginebra 2011; Zhang et al. 2014; Dele-Afolabi et al. 2018a, 2021). In this work, we focused in evaluating the tensile strength, by diametral compression test, of the biomaterial produced here. The tensile strength for A0PE was 14.37 ± 2.9 MPa, while for A15PE it was 5.89 ± 0.4 MPa (Fig. 1), the Pearson correlation value between the open porosity and the tensile strength was − 0.97, indicating a strong inverse correlation. The values obtained are comparable to the tensile strength of the human trabecular bone (bones with a porosity between 30 and 90%), which are between 1 and 5 MPa (Røhl et al. 1991; Wagoner Johnson and Herschler 2011); thus, the materials produced here can be potential substitutes for this type of bone.

Figure 2 shows the μCT images (Fig. 2a) and micrographs obtained by SEM of the substrates (Fig. 2b). It is observed that the substrates A5PE, A10PE, and A15PE have larger pores than those the A0PE, indicating that the beads inclusions contributed to the formation larger pores.

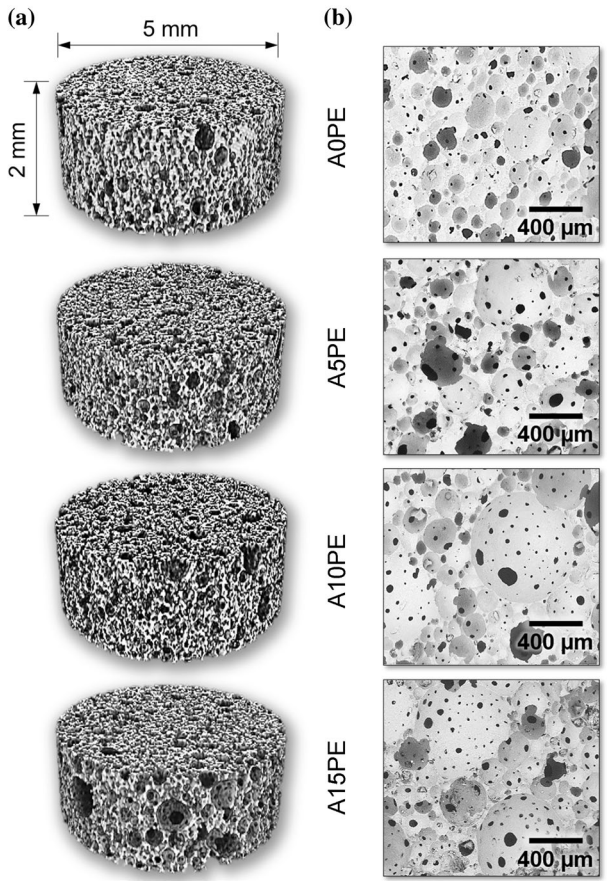

Fig. 2 **a** 3D µCT images and **b** SEM micrographs of the substrates with different additions of PE beads

Figure 3 shows the pore size distribution (according to their diameters) obtained by analysing 400 histological sections of 3D µCT for each condition studied. In general, the pore distribution profile was similar for the four conditions.

The foam-gelcasting method produces highly porous structures (Salomão et al. 2014; Sartori et al. 2018), but it can be seen that the addition of PE beads provided pores, in the structure, with a diameter range that is not observed in the sample without PE beads (500 and 2000 µm). Although the open porosity of the samples A5PE, A10PE, and A15PE did not show any differences between them (Fig. 1), the percentages of PE beads added created different volumes of macroporosity, as observed in Fig. 3. The larger pores resulting from the addition of PE beads replace those of smaller volume that would be formed by foam gelcasting without PE beads being added. Therefore, the open porosity between the A5PE, A10PE, and A15PE samples did not show a significant difference. However, this porosity could influence the deposition of the calcium phosphate layer on these surfaces. Besides that, a wide variation in pore size is interesting for a porous biomaterial, as each pore size allows different biological activities when inserted into the physiological environment (Annabi et al. 2010).

Characterisation of calcium phosphates formed in the biomimetic coating

The SEM micrographs of the A0PE, A5PE, A10PE, and A15PE samples, after 14 and 21 days of incubation, are shown in Fig. 4. In general, the structures emerging on the substrate's surfaces of all conditions studied calcium phosphate crystals, as showed the EDS results in Fig. S1 of the Supplementary Material. It is observed for all substrates, regardless of the incubation time.

The clusters observed in the micrographs (e.g. as highlighted with an arrow in Fig. 4 insets) are starting points of new layers deposition. Those clusters are also filling the pores creating a tri-dimensional calcium phosphate network throughout the substrates. This network would be beneficial since calcium phosphates are precursors of bone formation in the osteoconduction and osteoinduction processes. Thus, the network will stimulate and facilitate the formation of bone tissue throughout the substrates (Shavandi et al. 2015; Hesaraki 2016; Ebrahimi et al. 2017).

Figure 5a shows the second derivative of the absorption spectrum of NIR, and Fig. 5b shows the absorption spectrum of NIR, from the surface of A15PE covered with phosphate after 21 days in SBF, in the region between 4000 and 7000 cm^{-1}. In this interval, bands referring to calcium phosphates and Al_2O_3 are present. The spectral range from 4630 to 5430 cm^{-1} highlighted in Fig. 5c was treated mathematically (deconvolution) to distinguish the bands referring to calcium phosphates (bands in blue) and alumina (bands in red). As a result of the lesser interference of signals related to free water present on the surface of the samples, this

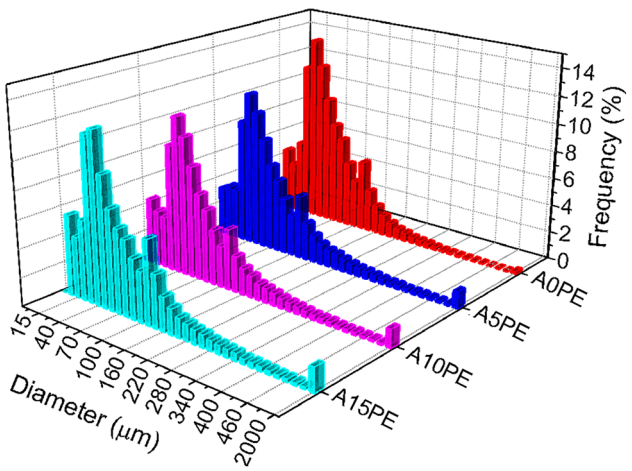

Fig. 3 Pore size distribution of the substrates with different amounts of PE beads

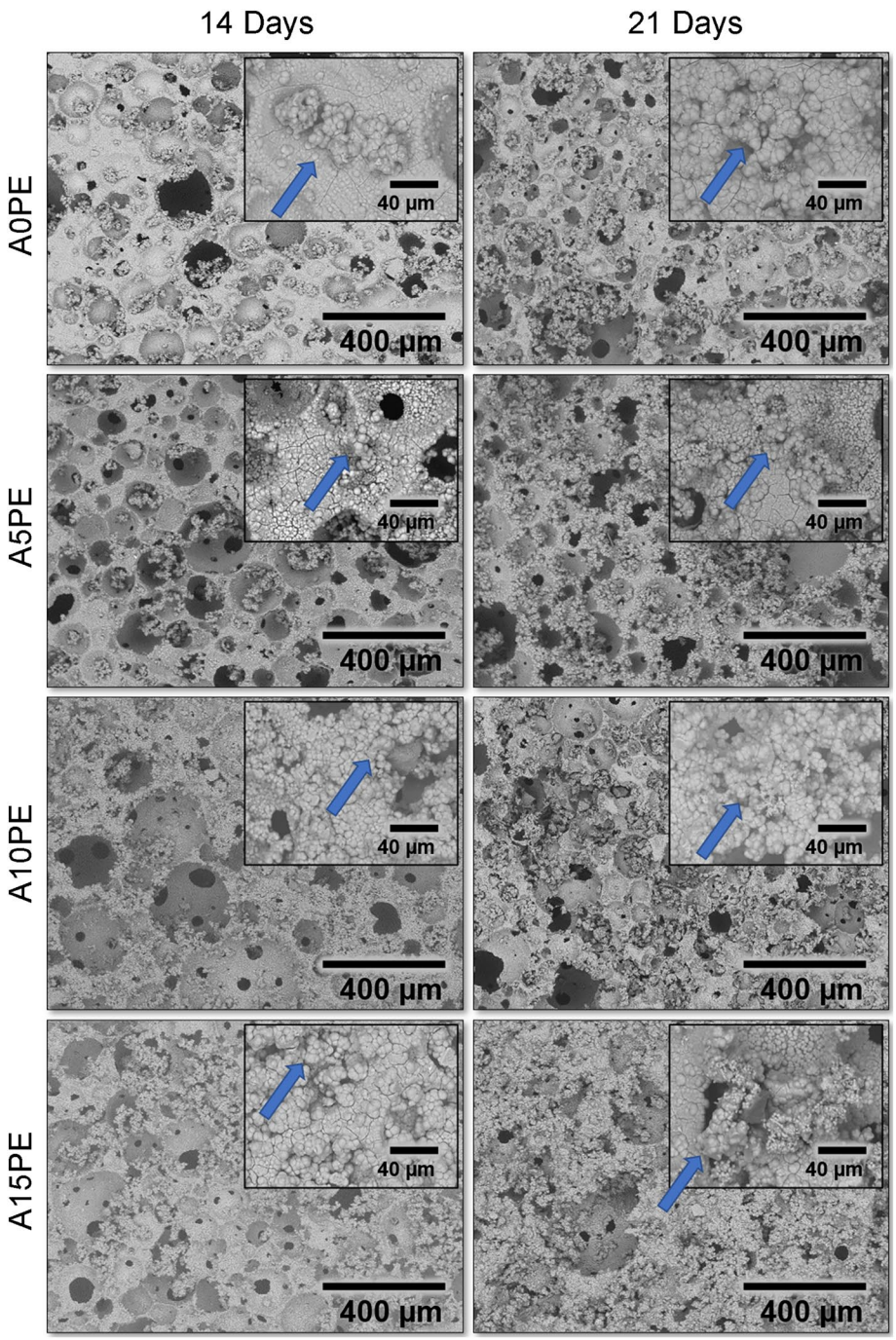

Fig. 4 SEM micrographs of the samples surface with different additions of PE beads covered biomimetically for 14 and 21 days, and insets with higher magnification for each condition

interval was chosen to quantify the deposited phosphates. The entire procedure was also carried out for the other conditions studied.

The bands in the NIR spectra are the result of combinations and overtones of the fundamental stretching (ν) and bending (δ) vibration bands of the middle infrared region (Workman and Weyer 2012). The attribution in the deconvolved NIR spectra was made by calculating the vibrational peaks from the values of stretching and bending vibrations of alumina and calcium phosphate in the region in the medium infrared. The following bands were used for Al_2O_3: O–H stretch of water physically adsorbed to Al^{3+} ($\nu_1 = \sim 3484.3\ cm^{-1}$), bend of Al–O–H ($\delta_a = \sim 1643.7$ and $\delta_b = \sim 1395.9\ cm^{-1}$), and stretch of Al–O ($\nu_3 = \sim 839.8\ cm^{-1}$) (Sarkar et al. 2007; Sartori et al. 2018). Calcium phosphate bands were calculated from the stretch of PO–H ($\nu_1 = \sim 3572\ cm^{-1}$), symmetrical stretch of P–O ($\nu_2 = \sim 960\ cm^{-1}$),bend of O–P–O (doubly degenerated bending mode) ($\delta_{1a} = \sim 472$ and $\delta_{1b} = 462\ cm^{-1}$), asymmetrical stretch of P–O ($\nu_{3a} = \sim 1087$, $\nu_{3b} = \sim 1046$

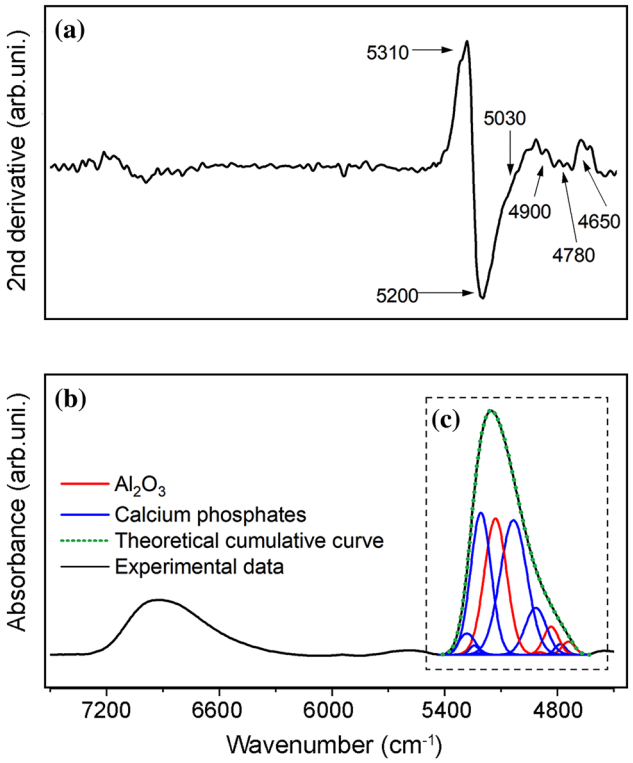

Fig. 5 **a** Second derivative of the spectrum, **b** NIR spectrum of the A15PE surface after 21 days of incubation, and (c) illustration of the "deconvolved analytical curves", where the blue bands represent the calcium phosphates and the red ones the Al_2O_3

and $\nu_{3c} = \sim 1032\ cm^{-1}$)and bend of O–P–O (triply degenerated bending mode) ($\delta_{2a} = \sim 602$, $\delta_{2b} = \sim 574$ and $\delta_{2c} = \sim 561\ cm^{-1}$) (Sureshbabu et al. 2012; Reddy et al. 2014; Sartori et al. 2018).

The substrates covered with calcium phosphates for all conditions studied showed NIR spectra with similar spectral profiles. The predominance of phosphate bands over Al_2O_3 (in all spectra) highlights the significant deposition of phosphates on surfaces. Table S1 (Supplementary Material) presents a description of the combined bands of the NIR spectra between 5430 and 4630 cm^{-1} on the surface of the substrate covered with calcium phosphates, also in the Supplementary Material more details about NIR data treatment are given. The position of the bands was obtained from the second derivative of the spectra (Fig. 5b). The quantification of calcium phosphates deposited on the surface of the substrate was performed from the absolute areas obtained from the deconvolved bands (Fig. 5c) (Czarnik-Matusewicz et al. 2005; Brangule and Gross 2015; Kolmas et al. 2015; dos Santoset al. 2017; Sartori et al. 2018).

In general, a tendency was observed: the greater the inclusion of PEbeads (the greater the porosity of the substrate), the greater the amount of calcium phosphates formed, regardless of the incubation period. It should be noted that the amount of phosphate formed in A5PE was slightly higher than in A10PE (for both incubation periods). This behaviour can be attributed to the similar total porosities of the two conditions (Fig. 1).

NIR spectroscopy makes it possible to relate and quantify the phosphates formed on the surfaces of the substrates. However, to identify the crystalline phases of calcium phosphates formed during the coating, XRD was used. Figure 6a shows the second derivative of the diffractogram, and Fig. 6b shows the A15PE diffractogram after 21 days of biomimetic coating, in the range of 26.8º–34.6º. The curves obtained by deconvolution of the diffractograms were related to the Miller index (hkl) for each phase of calcium phosphate, according to the database provided by the Joint Committee on Powder Diffraction Studies (JCPDS) (Joint Committee on Powder Diffraction Standards 2017). The entire procedure was also carried out for the other conditions studied.

Overall, five different phases of calcium phosphates were suggested for all conditions studied: HAp crystals in the planes (002), (210), (300), (113), (111), (102), (112) and (211); α-TCP in planes (241), (151), (511), (170), (113), (150), (312) and (402); β-TCP in planes (024), (306), (202), (150), (128), (210), (306) and (1112); TTCP in planes (-121), (200), (031), (211), (221), (1010), (112) and (113).

The relationship between the percentages present in each phase (obtained by the XRD technique) and the total absolute phosphate areas (obtained by the NIR technique) allows semi-quantitative analysis of each incubation period. Therefore, Fig. 7 shows the percentage suggested of crystalline phases in relation to the total absolute areas of calcium phosphates for the different conditions studied.

Regarding the phases observed, there was more α-TCP in the samples with 14 days of incubation than the ones with 21 days. On the other hand, the samples with 21 days of incubation presented more HAp, TTCP, and β-TCP compared to the ones with 14 days. The formation of the HAp and TTCP is related to the consumption of the α-TCP, due to the higher value of Ca/P ratio that HAp and TTCP have in comparison with α-TCP (HAp = 1.67, TTCP = 2.0, and α-TCP = 1.5 (Dorozhkin 2010)). In general, at 14 days of incubation, there is a higher amount of TTCP when compared to the β-TCP ($r_{TTCP/\beta-TCP} = -0.98$).This shows that 14 days is a satisfactory incubation period as it provides the production of calcium phosphates with higher Ca/P ratio values.

The high correlation between open porosity and the β-TCP phase ($r_{openporosity/\beta-TCP} = 0.95$) suggests that the increase in open porosity may have provided the formation of a new layer of calcium phosphate on top of a first layer previously deposited. The samples A5PE, A10PE, and A15PE, with 21 days of incubation, in addition to having a higher amount of HAp and TTCP, also presented a higher amount of β-TCP (Ca/P ratio = 1.5 (Dorozhkin 2010)) than

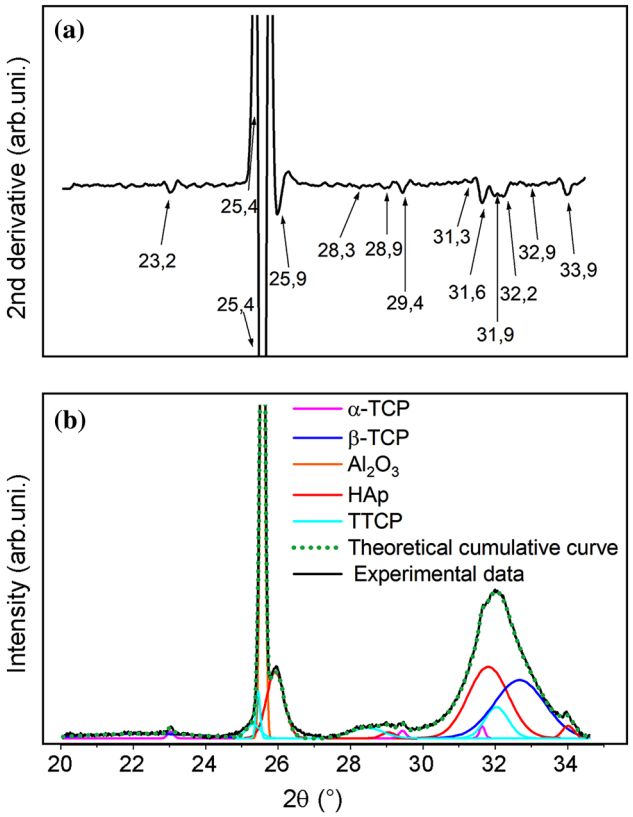

Fig. 6 **a** Second derivative of the XRD diffractogram and **b** diffractogram of the A15PE surface after 21 days of incubation with an illustration of the "deconvolved analytical curves", where each colour represents the different phases of calcium phosphates

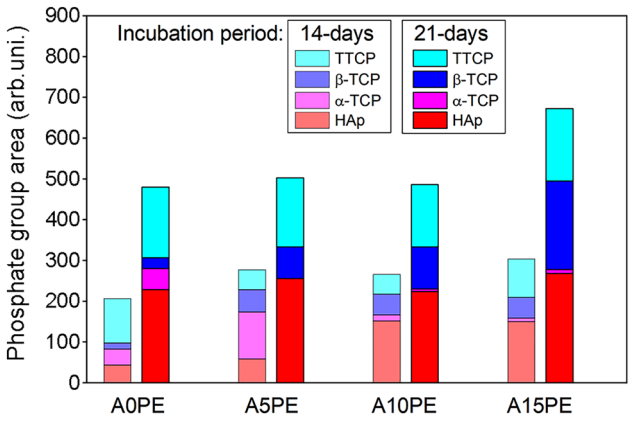

Fig. 7 Quantities of the calcium phosphate phases in the Al_2O_3 substrates with different additions of PE beads coated biomimetically for 14 and 21 days

the same conditions in 14 days of incubation. Thus, the addition of PE beads, and consequently higher open porosity, can influence some local characteristics, already mentioned, which may end up influencing the deposition mechanisms of Ca and P.

The main advantage of identifying and quantifying each phosphate phase formed in the different incubation periods is to allow an understanding of how the biomaterial can behave in the organism, since each phase presents different degrees of biodegradation (Habraken et al. 2016; Dorozhkin 2016; Zyman et al. 2017; Zhang et al. 2019). For example, HAp has a lower biodegradation rate compared to β-TCP, so it stays in the body for longer periods (Shavandi et al. 2015; Ebrahimi et al. 2017).Thus, knowing which phase presents the majority in the biomaterial produced, it is possible to determine in which application the biomaterial will perform better (Arjunan et al. 2022). In addition to determining the amount of calcium phosphates that the material contains, it is also possible to orientate the production of the desired phosphate phase by controlling the process parameters, such as the incubation time and porosity (dos Santos et al. 2017, 2018; Sartori et al. 2018).

Conclusions

Here, we showed that the open porosity has an influence on the phase formation of calcium phosphates obtained by the biomimetic method. Adding different amounts of PE beads with the gelcasting technique produced substrates with different open porosities and also in their interconnectivity. The phases more favourable with an increase in open porosity were HAp and β-TCP. Furthermore, the incubation time and the porosity of the substrate (surface area) can also influence the amount of calcium phosphates formed.

Supplementary Information The online version contains supplementary material available at https://doi.org/10.1007/s40204-022-00193-8.

Funding This study was financed by the National Council for Scientific and Technological Development (CNPq) [151281/2015-7; 102905/2015-0].

Declarations

Conflict of interest The authors declare that they have no conflict of interest.

Ethical approval This article does not contain any studies with human participants or animals performed by any of the authors.

References

Abe Y, Kokubo T, Yamamuro T (1990) Apatite coating on ceramics, metals and polymers utilizing a biological process. J Mater Sci Mater Med 1:233–238. https://doi.org/10.1007/BF00701082

Annabi N, Nichol JW, Zhong X et al (2010) Controlling the porosity and microarchitecture of hydrogels for tissue engineering. Tissue Eng Part B Rev 16:371–383. https://doi.org/10.1089/ten.teb.2009.0639

Arabnejad S, Burnett Johnston R, Pura JA et al (2016) High-strength porous biomaterials for bone replacement: a strategy to assess the interplay between cell morphology, mechanical properties, bone ingrowth and manufacturing constraints. Acta Biomater 30:345–356. https://doi.org/10.1016/j.actbio.2015.10.048

Arjunan A, Baroutaji A, Robinson J et al (2022) Future directions and requirements for tissue engineering biomaterials. Encyclopedia of smart materials. Elsevier, Amsterdam, pp 195–218

ASTM D3967-95a (2001) Splitting Tensile Strength of Intact Rock Core Specimens. ASTM Int

Barrere F, van Blitterswijk C, de Groot K, Layrolle P (2002a) Influence of ionic strength and carbonate on the Ca-P coating formation from SBF×5 solution. Biomaterials 23:1921–1930. https://doi.org/10.1016/S0142-9612(01)00318-0

Barrere F, van Blitterswijk C, de Groot K, Layrolle P (2002b) Nucleation of biomimetic Ca–P coatings on Ti_6Al_4V from a SBF×5 solution: influence of magnesium. Biomaterials 23:2211–2220. https://doi.org/10.1016/S0142-9612(01)00354-4

Belwanshi M, Jayaswal P, Aherwar A (2021) A study on tribological effect and surface treatment methods of Bio-ceramics composites. Mater Today Proc 44:4131–4137. https://doi.org/10.1016/j.matpr.2020.10.458

Bohner M, Santoni BLG, Döbelin N (2020) β-tricalcium phosphate for bone substitution: synthesis and properties. Acta Biomater 113:23–41. https://doi.org/10.1016/j.actbio.2020.06.022

Böke F, Schickle K, Fischer H (2014) Biological activation of inert ceramics: recent advances using tailored self-assembled monolayers on implant ceramic surfaces. Materials (basel) 7:4473–4492. https://doi.org/10.3390/ma7064473

Brangule A, Gross KA (2015) Importance of FTIR spectra deconvolution for the analysis of amorphous calcium phosphates. IOP Conf Ser Mater Sci Eng. https://doi.org/10.1088/1757-899X/77/1/012027

Canal C, Ginebra MP (2011) Fibre-reinforced calcium phosphate cements: a review. J Mech Behav Biomed Mater 4:1658–1671. https://doi.org/10.1016/j.jmbbm.2011.06.023

Chen Q, Zhu C, Thouas GA (2012) Progress and challenges in biomaterials used for bone tissue engineering: bioactive glasses and elastomeric composites. Prog Biomater 1:2. https://doi.org/10.1186/2194-0517-1-2

Czarnik-Matusewicz B, Pilorz S, Hawranek JP (2005) Temperature-dependent water structural transitions examined by near-IR and mid-IR spectra analyzed by multivariate curve resolution and two-dimensional correlation spectroscopy. Anal Chim Acta 544:15–25. https://doi.org/10.1016/j.aca.2005.04.040

da Sartori TAIC, Ferreira JA, Osiro D et al (2018) Formation of different calcium phosphate phases on the surface of porous Al_2O_3-ZrO_2nanocomposites. J Eur Ceram Soc 38:743–751. https://doi.org/10.1016/j.jeurceramsoc.2017.09.014

Dehestani M, Ilver L, Adolfsson E (2012) Enhancing the bioactivity of zirconia and zirconia composites by surface modification. J Biomed Mater Res Part B Appl Biomater 100B:832–840. https://doi.org/10.1002/jbm.b.32647

Dele-Afolabi TT, Hanim MAA, Norkhairunnisa M et al (2017) Investigating the effect of porosity level and pore former type on the mechanical and corrosion resistance properties of agro-waste shaped porous alumina ceramics. Ceram Int 43:8743–8754. https://doi.org/10.1016/j.ceramint.2017.03.210

Dele-Afolabi T, Azmah Hanim MA, Mazlan N et al (2018a) Effect of agro-waste pore formers on the microstructure, hardness, and tensile properties of porous alumina ceramics. Int J Appl Ceram Technol 15:1060–1071. https://doi.org/10.1111/ijac.12874

Dele-Afolabi TT, Azmah Hanim MA, Norkhairunnisa M et al (2018b) Significant effect of rice husk and sugarcane bagasse pore formers on the microstructure and mechanical properties of porous Al_2O_3/Ni composites. J Alloys Compd 743:323–331. https://doi.org/10.1016/j.jallcom.2018.01.230

Dele-Afolabi TT, Azmah Hanim MA, Ojo-Kupoluyi OJ et al (2021) Tailored pore structures and mechanical properties of porous alumina ceramics prepared with corn cob pore-forming agent. Int J Appl Ceram Technol 18:244–252. https://doi.org/10.1111/ijac.13621

Dorozhkin SV (2010) Bioceramics of calcium orthophosphates. Biomaterials 31:1465–1485. https://doi.org/10.1016/j.biomaterials.2009.11.050

Dorozhkin SV (2012) Calcium orthophosphate coatings, films and layers. Prog Biomater 1:1. https://doi.org/10.1186/2194-0517-1-1

Dorozhkin SV (2016) Calcium orthophosphates ($CaPO_4$): occurrence and properties. Prog Biomater 5:9–70. https://doi.org/10.1007/s40204-015-0045-z

Ebrahimi M, Botelho MG, Dorozhkin SV (2017) Biphasic calcium phosphates bioceramics (HA/TCP): Concept, physicochemical properties and the impact of standardization of study protocols in biomaterials research. Mater Sci Eng C 71:1293–1312. https://doi.org/10.1016/j.msec.2016.11.039

Faga MG, Vallée A, Bellosi A et al (2012) Chemical treatment on alumina—zirconia composites inducing apatite formation with maintained mechanical properties. J Eur Ceram Soc 32:2113–2120. https://doi.org/10.1016/j.jeurceramsoc.2011.12.020

Gadaleta SJ, Paschalis EP, Betts F et al (1996) Fourier transform infrared spectroscopy of the solution-mediated conversion of amorphous calcium phosphate to hydroxyapatite: new correlations between X-ray diffraction and infrared data. Calcif Tissue Int 58:9–16. https://doi.org/10.1007/s002239900004

Habraken W, Habibovic P, Epple M, Bohner M (2016) Calcium phosphates in biomedical applications: Materials for the future? Mater Today 19:69–87. https://doi.org/10.1016/j.mattod.2015.10.008

Hesaraki S (2016) Feasibility of alumina and alumina-silica nanoparticles to fabricate strengthened betatricalcium phosphate scaffold with improved biological responses. Ceram Int 42:7593–7604. https://doi.org/10.1016/j.ceramint.2016.01.167

Joint Committee on Powder Diffraction Standards J Joint Committee on Powder Diffraction Standards, JCPDS. International Center for Diffraction Data, and American Society for Testing and Materials, Powder Diffraction File (2017) Cards Numbers: 09-432, 73-1731, 09-348, 09-169, 25-1137 e 79-0423

Karageorgiou V, Kaplan D (2005) Porosity of 3D biomaterial scaffolds and osteogenesis. Biomaterials 26:5474–5491. https://doi.org/10.1016/j.biomaterials.2005.02.002

Karampour H, Parsa MA, Moghadam AH et al (2022) Facile solution-based synthesis of impurity-free hydroxyapatite nanocrystals at ambient conditions. J Mater Res Technol 16:656–674. https://doi.org/10.1016/j.jmrt.2021.12.028

Karczewski K, Stepniowski W, Salerno M (2017) Amino acids aided sintering for the formation of highly porous FeAl intermetallic alloys. Materials (basel) 10:746. https://doi.org/10.3390/ma10070746

Kokubo T (1998) Apatite formation on surfaces of ceramics, metals and polymers in body environment. Acta Mater 46:2519–2527. https://doi.org/10.1016/S1359-6454(98)80036-0

Kolmas J, Marek D, Kolodziejski W (2015) Near-infrared (NIR) spectroscopy of synthetic hydroxyapatites and human dental tissues. Appl Spectrosc 69:902–912. https://doi.org/10.1366/14-07720

Kolos E, Ruys AJ (2015) Biomimetic coating on porous alumina for tissue engineering: characterisation by cell culture and confocal microscopy. Materials (basel) 8:3584–3606. https://doi.org/10.3390/ma8063584

Nunes FC, Maia MA, Santos KH et al (2021) Influence of Sr^{2+} in calcium phosphates formation on the surface of Al_2O_3/ZrO_2nanocomposites. Ceram Int 47:30685–30690. https://doi.org/10.1016/j.ceramint.2021.07.247

Petit C, Meille S, Maire E et al (2016) Mechanical behaviour of a β-TCP ceramic with a random porosity: Study of the fracture path with X-ray tomography. J Eur Ceram Soc 36:3225–3233. https://doi.org/10.1016/j.jeurceramsoc.2016.05.001

Rambo CR, Muller FA, Muller L et al (2006) Biomimetic apatite coating on biomorphous alumina scaffolds. Mater Sci Eng C 26:92–99. https://doi.org/10.1016/j.msec.2005.06.003

Reddy GU, Reddy TR, Padmalatha KS (2014) Synthesis XRD TEM and optical absorption spectroscopic characterization of copper doped nano apatite. Prog NanotechnolNanomater 3:19–25

Røhl L, Larsen E, Linde F et al (1991) Tensile and compressive properties of cancellous bone. J Biomech 24:1143–1149. https://doi.org/10.1016/0021-9290(91)90006-9

Sabree I, Gough JE, Derby B (2015) Mechanical properties of porous ceramic scaffolds: influence of internal dimensions. Ceram Int 41:8425–8432. https://doi.org/10.1016/j.ceramint.2015.03.044

Salerno M, Loria P, Matarazzo G et al (2016) Surface morphology and tooth adhesion of a novel nanostructured dental restorative composite. Materials (basel) 9:1–8. https://doi.org/10.3390/ma9030203

Salomão R, Cardoso PH, Brandi J (2014) Gelcasting porous alumina beads of tailored shape and porosity. Ceram Int 40:16595–16601. https://doi.org/10.1016/j.ceramint.2014.08.017

Santos KH, Ferreira JA, Osiro D et al (2017) Influence of different chemical treatments on the surface of Al_2O_3/ZrO_2nanocomposites during biomimetic coating. Ceram Int 43:4272–4279. https://doi.org/10.1016/j.ceramint.2016.12.069

Santos KH, Ferreira JA, Osiro D et al (2018) Plasma surface treatments of Al_2O_3/ZrO_2nanocomposites and their influence on the formation and adhesion of calcium phosphates. Appl Surf Sci 456:552–560. https://doi.org/10.1016/j.apsusc.2018.06.188

Santos KH, Ferreira JA, Osiro D et al (2020) Influence of the cold plasma treatment on the Al_2O_3/ZrO_2 nanocomposites surfaces. Appl Surf Sci 531:147206. https://doi.org/10.1016/j.apsusc.2020.147206

Sarkar D, Mohapatra D, Ray S et al (2007) Synthesis and characterization of sol-gel derived ZrO_2 doped Al_2O_3nanopowder. Ceram Int 33:1275–1282. https://doi.org/10.1016/j.ceramint.2006.05.002

Schröter L, Kaiser F, Stein S et al (2020) Biological and mechanical performance and degradation characteristics of calcium phosphate cements in large animals and humans. Acta Biomater 117:1–20. https://doi.org/10.1016/j.actbio.2020.09.031

Seyedlar RM, Rezvani M, Barari S et al (2019) Synthesis of plate-like β-tricalcium phosphate nanoparticles and their efficiency in remineralization of incipient enamel caries. Prog Biomater 8:261–276. https://doi.org/10.1007/s40204-019-00126-y

Shavandi A, Bekhit AEA, Ali MA et al (2015) Development and characterization of hydroxyapatite/β -TCP/chitosan composites for tissue engineering applications. Mater Sci Eng C 56:481–493. https://doi.org/10.1016/j.msec.2015.07.004

Silva ADR, Rigoli WR, Osiro D et al (2018) Surface modification using the biomimetic method in alumina-zirconia porous ceramics obtained by the replica method. J Biomed Mater Res Part B Appl Biomater 106:2615–2624. https://doi.org/10.1002/jbm.b.34078

Silva ADR, Rigoli WR, Mello DCR et al (2019) Porous alumina scaffolds chemically modified by calcium phosphate minerals and their application in bone grafts. Int J Appl Ceram Technol 16:562–573. https://doi.org/10.1111/ijac.13153

Sureshbabu S, Komath M, Varma HK (2012) In situ formation of hydroxyapatite - alpha tricalcium phosphate biphasic ceramics with higher strength and bioactivity. J Am Ceram Soc 95:915–924. https://doi.org/10.1111/j.1551-2916.2011.04987.x

Tang X, Mao L, Liu J et al (2016) Fabrication, characterization and cellular biocompatibility of porous biphasic calcium phosphate bioceramic scaffolds with different pore sizes. Ceram Int 42:15311–15318. https://doi.org/10.1016/j.ceramint.2016.06.172

Thavornyutikarn B, Chantarapanich N, Sitthiseripratip K et al (2014) Bone tissue engineering scaffolding: computer-aided scaffolding techniques. Prog Biomater 3:61–102. https://doi.org/10.1007/s40204-014-0026-7

Toccafondi C, Dante S, Reverberi AP, Salerno M (2015) Biomedical applications of anodic porous alumina. Curr Nanosci 11:572–580. https://doi.org/10.2174/1573413711666150415225541

Uchida M, Kim H, Kokubo T et al (2002) Apatite-forming ability of a zirconia/alumina nano-composite induced by chemical treatment. J Biomed Mater Res Part A 60:277–282. https://doi.org/10.1002/jbm.10071

Wagoner Johnson AJ, Herschler BA (2011) A review of the mechanical behavior of CaP and CaP/polymer composites for applications in bone replacement and repair. Acta Biomater 7:16–30. https://doi.org/10.1016/j.actbio.2010.07.012

Wang Y (2016) Bioadaptability: an innovative concept for biomaterials. J Mater Sci Technol 32:801–809. https://doi.org/10.1016/j.jmst.2016.08.002

Workman J Jr, Weyer L (2012) Pratical guide and spectral atlas for interpretive near-infrared spectroscopy, 2nd edn. CRC, New York

Xie R, Zhang D, Zhang X et al (2012) Gelcasting of alumina ceramics with improved green strength. Ceram Int 38:6923–6926. https://doi.org/10.1016/j.ceramint.2012.05.027

Xu W, Tian J, Liu Z et al (2019) Novel porous $Ti_{35}Zr_{28}Nb$ scaffolds fabricated by powder metallurgy with excellent osteointegration ability for bone-tissue engineering applications. Mater Sci Eng C 105:110015. https://doi.org/10.1016/j.msec.2019.110015

Yoo D (2013) New paradigms in hierarchical porous scaffold design for tissue engineering. Mater Sci Eng C 33:1759–1772. https://doi.org/10.1016/j.msec.2012.12.092

Zhang J, Liu W, Schnitzler V et al (2014) Calcium phosphate cements for bone substitution: Chemistry, handling and mechanical properties. Acta Biomater 10:1035–1049. https://doi.org/10.1016/j.actbio.2013.11.001

Zhang Y, Shao H, Lin T et al (2019) Effect of Ca/P ratios on porous calcium phosphate salt bioceramic scaffolds for bone engineering by 3D gel-printing method. Ceram Int 45:20493–20500. https://doi.org/10.1016/j.ceramint.2019.07.028

Zyman Z, Goncharenko A, Rokhmistrov D (2017) Kinetics and mechanisms of the transformation of precipitated amorphous calcium phosphate with a Ca/P ratio of 1:1 to calcium pyrophosphates. J Cryst Growth 478:117–122. https://doi.org/10.1016/j.jcrysgro.2017.08.031